


# Majorana gap formation in the anisotropic Kitaev model with ordered flux configuration

Akihiro Hashimoto,<sup>1</sup> Yuta Murakami<sup>2</sup>, and Akihisa Koga<sup>1</sup>

<sup>1</sup>*Department of Physics, Tokyo Institute of Technology, Meguro, Tokyo 152-8551, Japan*

<sup>2</sup>*Center for Emergent Matter Science, RIKEN, Wako 351-0198, Japan*

 (Received 7 March 2023; accepted 11 May 2023; published 23 May 2023)

We study the Kitaev model with direction-dependent interactions to investigate how the flux configuration and/or the anisotropy in the exchanges affect the Majorana excitations. It is found that the triangular flux configurations with unit length  $q$  induce the quantum spin liquid states with gapped Majorana excitations. Systematic numerical calculations demonstrate that  $(q-1)(q-2)/2$  gapped states bounded by gapless states are realized in the vicinity of the isotropic limit. The induced gapped quantum spin liquid states are not adiabatically connected to the gapped one realized in the large anisotropic limit. Therefore, these two states are distinct from each other. The nature of the gapped states can be explained by the fact that the hybridization between the gapless points, which originates from the superlattice potential due to the flux configuration, opens the gap in the Majorana excitations.

DOI: [10.1103/PhysRevB.107.174428](https://doi.org/10.1103/PhysRevB.107.174428)

## I. INTRODUCTION

Over the last few decades, the quantum spin liquid state has attracted much interest. One of the interesting examples to realize it is the Kitaev model [1], whose ground state and finite-temperature properties have recently been studied in detail [2–12]. This model is composed of the direction-dependent Ising interactions ( $J_x, J_y, J_z$ ), which are schematically shown in Fig. 1(a). Due to the existence of the local conserved quantity on each plaquette, the Kitaev model is solvable and the spin degrees of freedom is fractionalized into itinerant Majorana fermions and local fluxes. It is known that, in the ground state, the flux degrees of freedom is frozen and the quantum spin liquid state is realized. Low-energy properties are then described by the itinerant Majorana fermions. When the magnitudes of three interactions  $J_x, J_y$ , and  $J_z$  are the same, which is called the “isotropic” case, the Dirac cone type dispersion appears in the Majorana excitations and the system is gapless. It is also known that the topologically protected quantum spin liquid state is realized when the magnetic field is applied to the isotropic system [1], which makes the Kitaev system more interesting. Magnetic properties inherent in the Kitaev model have experimentally been examined in the candidate materials such as  $A_2\text{IrO}_3$  ( $A = \text{Li, Na, H}_{3/2}\text{Li}_{1/2}$ ) [13–18],  $\alpha\text{-RuCl}_3$  [19,20], and  $\text{Na}_3\text{Co}_2\text{AO}_6$  ( $A = \text{Sb, Te}$ ) [21]. In particular, in the material  $\alpha\text{-RuCl}_3$ , a half-integer quantized plateau has been reported in the thermal quantum Hall experiments [22–25], which may be associated with a topologically protected chiral Majorana edge mode. Some conflicting results have also been reported [26–28], stimulating further investigations on topological properties in the system. As for the bulk properties, the spin transport mediated by the itinerant Majorana fermions have theoretically been discussed [29–31] although no experiments has been reported so far.

When a certain Ising interaction is much larger than the others (anisotropic case), the system should be described by

the toric code [32]. In this case, the quantum spin liquid state is realized with gapped Majorana excitations and Majorana correlations exponentially decay. Therefore, the system can be regarded as a Majorana insulator, in contrast to the isotropic case. It has been claimed that the anisotropy in the exchanges in the candidate materials can be controlled by the circularly polarized light field [33], which should allow us to control the motion of the Majorana fermions. Furthermore, the effects of the flux degrees of freedom on the Majorana excitations have recently been studied [28,34–38]. It has been

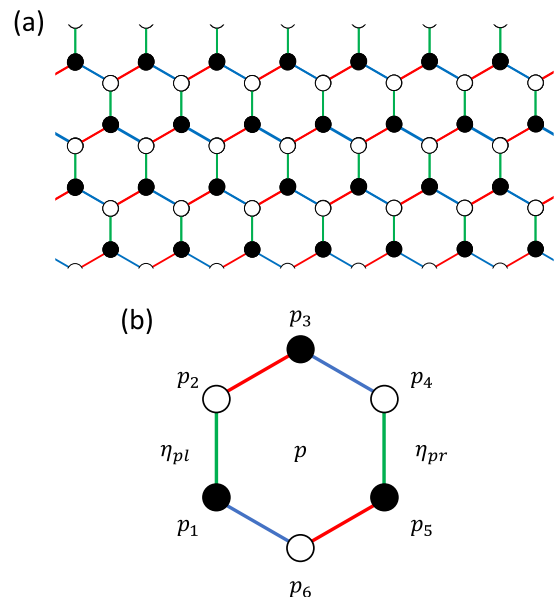


FIG. 1. (a) Kitaev model with direction-dependent Ising exchanges. Red, blue, and green lines represent the  $x$ ,  $y$ , and  $z$  bonds. (b) Plaquette with sites  $p_1, p_2, \dots, p_6$ .  $\eta_{pl}$  and  $\eta_{pr}$  indicate the local conserved quantities on the  $z$  bonds of the left and right edges on the plaquette  $p$ .

clarified that the gapped quantum spin liquid state is realized when the system has a certain flux configuration [39]. It has also been clarified that this gapped state is not adiabatically connected to the gapped one realized in the toric code [40]. This suggests that the flux configurations and/or anisotropy in the exchanges should play an important role for the Majorana excitations in the Kitaev model. It has also been discussed how the ordered flux configurations affect the Majorana Chern insulator [41–44]. It is instructive to clarify the nature of the gap formation in the Majorana excitation in the Kitaev model.

In this paper, we treat the anisotropic Kitaev model on the honeycomb lattice to clarify the effects of the triangular flux configurations and/or anisotropy in the exchange couplings on the Majorana excitations. Performing systematic calculations, we examine how the gap appears in the Majorana excitations. We clarify that the gapped quantum spin liquid states are induced by the periodic flux configurations and are not adiabatically connected to the gapped state described by the toric code.

This paper is organized as follows. In Sec. II, we introduce the anisotropic Kitaev model and explain our method to treat the flux configuration. By calculating the dispersion relations systematically, we obtain the lowest Majorana excitation (Majorana gap). Then, we discuss the Majorana gap formation in the system with the triangular flux configuration in Sec. III. A summary is given in the last section.

## II. MODEL AND METHOD

We consider the anisotropic Kitaev model, which is described by the following Hamiltonian as

$$H = -J_x \sum_{\langle i,j \rangle_x} S_i^x S_j^x - J_y \sum_{\langle i,j \rangle_y} S_i^y S_j^y - J_z \sum_{\langle i,j \rangle_z} S_i^z S_j^z, \quad (1)$$

where  $\langle i,j \rangle_\alpha$  stands for the nearest-neighbor pair on  $\alpha (= x, y, z)$  bonds.  $S_i^\alpha (= \frac{1}{2} \sigma_i^\alpha)$  is the  $\alpha$  component of the  $S = 1/2$  spin operator at the  $i$ th site and  $\sigma^\alpha$  is the  $\alpha$  component of the Pauli matrix.  $J_\alpha (> 0)$  is the ferromagnetic exchange coupling on the  $\alpha$  bond. The model is schematically shown in Fig. 1(a). One of the important features of this model is the existence of the local conserved quantity [1]. The local operator  $W_p$  on a plaquette  $p$  is defined by  $W_p = \sigma_{p_1}^x \sigma_{p_2}^y \sigma_{p_3}^z \sigma_{p_4}^x \sigma_{p_5}^y \sigma_{p_6}^z$ , where  $p_i$  ( $i = 1, 2, \dots, 6$ ) is the site on plaquette  $p$  [see Fig. 1(b)]. Since  $[W_p, W_{p'}] = 0$ ,  $[W_p, H] = 0$ , and  $W_p^2 = 1$ , the operator  $W_p$  is a local conserved quantity with eigenvalue  $w_p = \pm 1$ . Then, each eigenstate of the Kitaev Hamiltonian can be classified by the subspace with the set of  $w_p$ . It is known that the ground state is realized in the subspace with  $w_p = 1$  for each plaquette [45]. Therefore, one can regard a plaquette with  $w_p = -1$  as a flux and the subspace of the ground state as a flux-free one. We note that the existence of the local conserved quantities leads to the absence of the local moment and long-range spin-spin correlations in the system. Therefore, the quantum spin liquid is always realized for any flux configuration.

To discuss low-energy properties in the Kitaev model, we use the Jordan-Wigner transformation [46–48] and obtain the

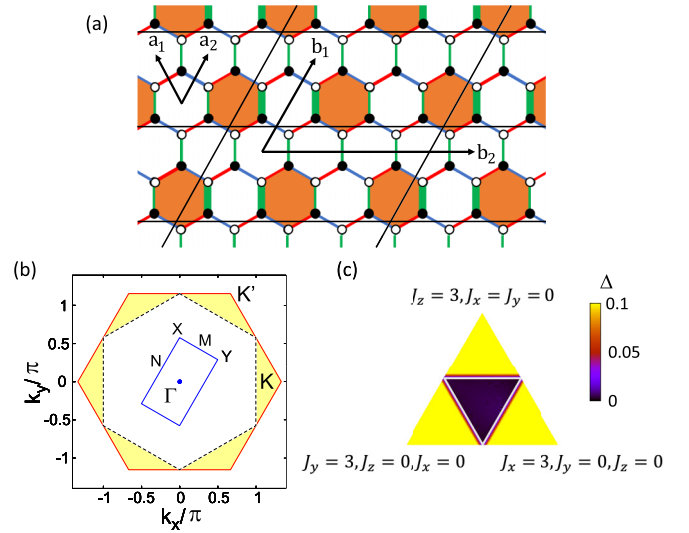


FIG. 2. (a) The flux configuration ( $q = 2$ ) and primitive vectors. (b) The red (blue) line shows the original (reduced) Brillouin zone in the Kitaev model. Shaded regions show the possible area of the gapless point  $k_G$  in the flux-free system (see text). (c) Majorana excitation gap in the flux-free system. The gapless state appears inside the triangle region specified by the white lines.

Hamiltonian in the Majorana representation as

$$H = -\frac{iJ_x}{4} \sum_{\langle rb,r'w \rangle_x} \gamma_{rb} \gamma_{r'w} - \frac{iJ_y}{4} \sum_{\langle rb,r'w \rangle_y} \gamma_{rb} \gamma_{r'w} - \frac{iJ_z}{4} \sum_r \eta_r \gamma_{rb} \gamma_{rw}, \quad (2)$$

where  $\gamma_{rb}$  ( $\bar{\gamma}_{rw}$ ) is the itinerant (localized) Majorana fermion operator at the black (white) site on the  $r$ th  $z$  bond and  $\eta_r = i\bar{\gamma}_{rb}\bar{\gamma}_{rw}$  [see Fig. 1(a)]. Since  $[\eta_r, \eta_{r'}] = 0$ ,  $[\eta_r, H] = 0$ , and  $\eta_r^2 = 1$ ,  $\eta_r$  is a  $Z_2$  local conserved quantity. It is known that  $W_p = \eta_{p_l} \eta_{p_r}$ , where  $p_l$  ( $p_r$ ) is the left (right)  $z$  bonds on plaquette  $p$ . Therefore, the flux configuration  $\{w_p\}$  can be represented by the configuration  $\{\eta_r\}$  instead. The ground

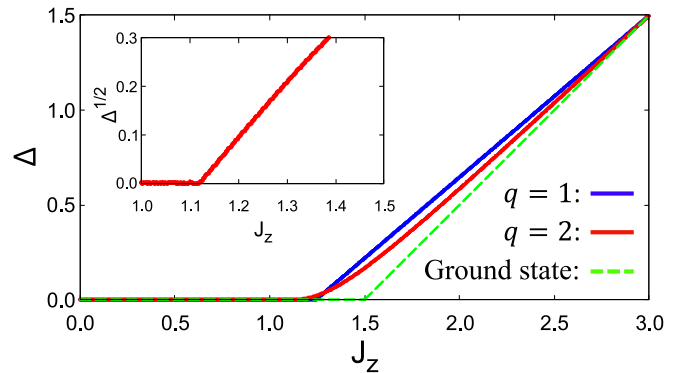


FIG. 3. Blue and red lines represent Majorana excitation gap  $\Delta$  in the systems with the flux configurations  $q = 1$  and  $q = 2$  under the conditions  $J_x + J_y + J_z = 3$  and  $J_x = J_y$ . The dashed line represents the results for the flux-free state. The inset shows  $\Delta^{1/2}$  as a function of  $J_z$  when  $q = 2$ .

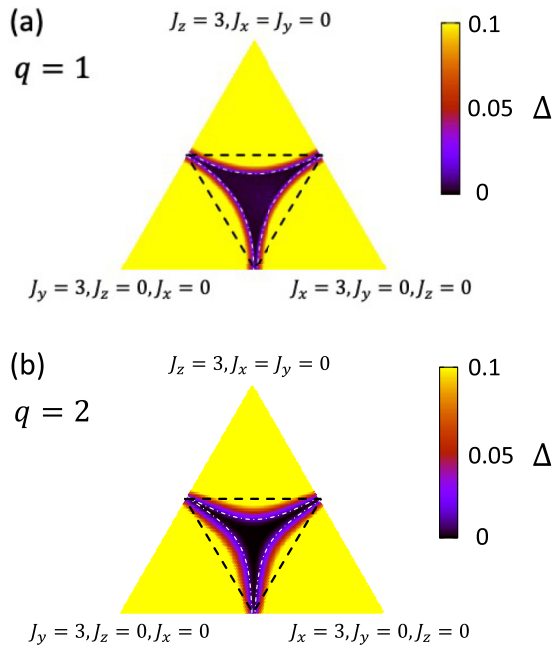


FIG. 4. Majorana excitation gap in the system with the flux configurations (a)  $q = 1$  and (b)  $q = 2$  on the plane  $J_x + J_y + J_z = 3$ .

state can be characterized by the subspace with  $\eta_r = 1$  for each  $z$  bond.

Ground state properties in the flux-free subspace are well examined [1]. The dispersion relation for itinerant Majorana fermions is given by

$$\epsilon(\mathbf{k}) = \frac{1}{2} |J_x \exp(i\mathbf{k} \cdot \mathbf{a}_2) + J_y \exp(i\mathbf{k} \cdot \mathbf{a}_1) + J_z|, \quad (3)$$

where  $\mathbf{a}_1$  and  $\mathbf{a}_2$  are primitive vectors of the honeycomb lattice [see Fig. 2(a)], and  $\mathbf{k}$  is the wave vector. In the isotropic case with  $J_x = J_y = J_z$ , the linear dispersion appears and the gapless points are located at the  $K$  and  $K'$  points in the Brillouin zone, as shown in Fig. 2(b). Introducing the anisotropy in the exchange, the gapless points gradually change. When the set of exchanges satisfies triangle inequalities [triangle region in the diagram shown in Fig. 2(c)],

$$J_x + J_y \geq J_z, \quad (4)$$

$$J_y + J_z \geq J_x, \quad (5)$$

$$J_z + J_x \geq J_y, \quad (6)$$

the system is gapless, and the gapless points take the inside of a certain region in the Brillouin zone shown as a shaded area in Fig. 2(b). On the other hand, when the exchanges are away from the triangle inequalities, the excitation gap appears in the Majorana excitation. In this case, the system should be adiabatically connected to that for the dimer limit ( $J_x = J_y = 0$ ), and thereby low-energy properties are effectively described by the toric code [32]. It is also known that Majorana excitations are controlled by not only the anisotropy in the exchanges, but also the flux configurations [39]. Therefore, it is necessary to clarify the gap formation in the Majorana systems and the role of flux configurations and/or anisotropy in the exchange.

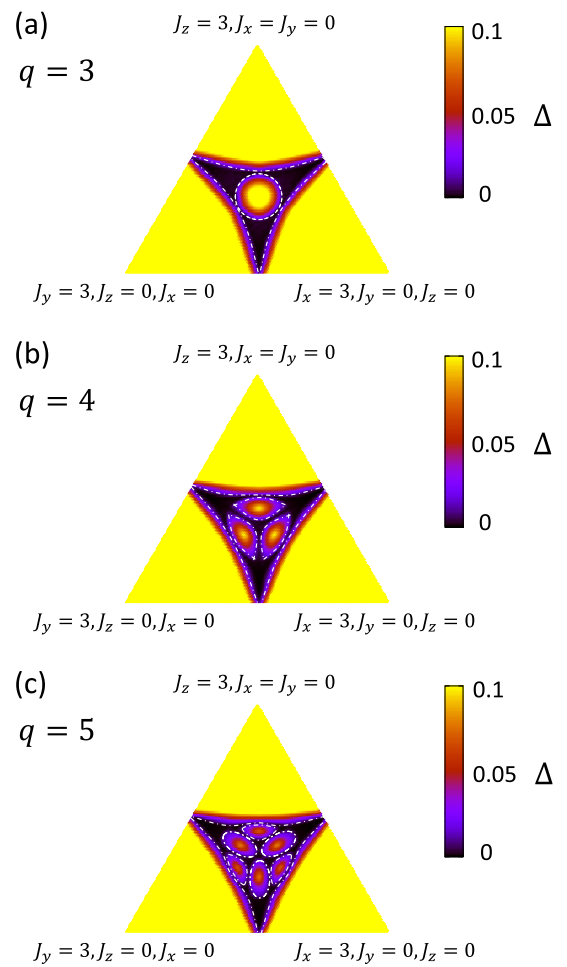


FIG. 5. Majorana excitation gap in the system with the flux configurations (a)  $q = 3$ , (b)  $q = 4$ , and (c)  $q = 5$  on the plane  $J_x + J_y + J_z = 3$ .

In this study, we focus on the triangular flux configurations, where the fluxes are periodically arranged in the honeycomb sheet, as shown in Fig. 2(a). This flux configuration is specified by its unit length  $q$ . We note that the Majorana Hamiltonian equation (2) is represented by the  $(2q^2 \times 2q^2)$

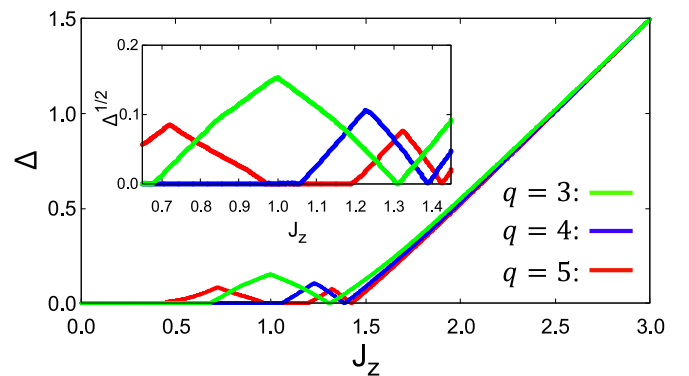


FIG. 6. Majorana excitation gap  $\Delta$  as a function of  $J_z$  under the condition  $J_x = J_y$ , when  $q = 3$  (green),  $q = 4$  (blue), and  $q = 5$  (red). Inset is the magnified figure around  $J_z = 1$ .

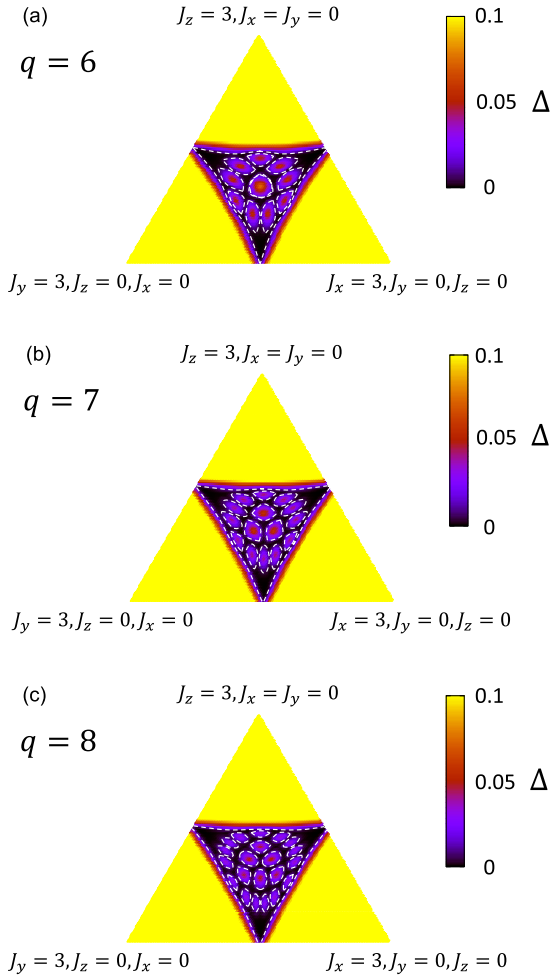


FIG. 7. Majorana excitation gap in systems with flux configurations  $q = 6, 7$ , and  $8$ .

matrices in the Fourier space. The flux-free configuration corresponds to the limit  $q \rightarrow \infty$ . When the triangular flux configuration is represented by the set of  $\{\eta_r\}$ , the unit cell is characterized by the primitive vectors  $\mathbf{b}_1 = q\mathbf{a}_2$  and  $\mathbf{b}_2 = -2q\mathbf{a}_1 + 2q\mathbf{a}_2$  [see Fig. 2(a)]. We should note that the unit cell specified by the  $\{\eta_r\}$  is different from the one by the flux. The set of  $\{\eta_r\}$  for the flux configuration  $q = 2$  is shown as the bold and thin lines on the  $z$  bonds. The Brillouin zone for the original Kitaev model is given by the hexagon in the Fourier space, and the reduced one for flux configurations  $q$  is given by the rectangle, as shown in Fig. 2(b). In the following, we study the Majorana excitation under the conditions  $J_x + J_y + J_z = 3$ . We note that, in the system with the triangular flux configuration, the model Hamiltonian equation (2) is symmetric under the exchange operation in  $\{J_x, J_y, J_z\}$ .

Before starting with discussions, we comment on magnetic properties in two limits of the system with the flux configuration  $q$ . When  $J_z$  is large, the system is reduced to the weakly coupled dimers, where the Majorana gap, which is defined by the lowest energy of the Majorana dispersion relation, is  $\Delta \sim J_z$  and the flux configuration is irrelevant. In this case, the effective Hamiltonian should be given by the fourth-order perturbation theory and the system is described

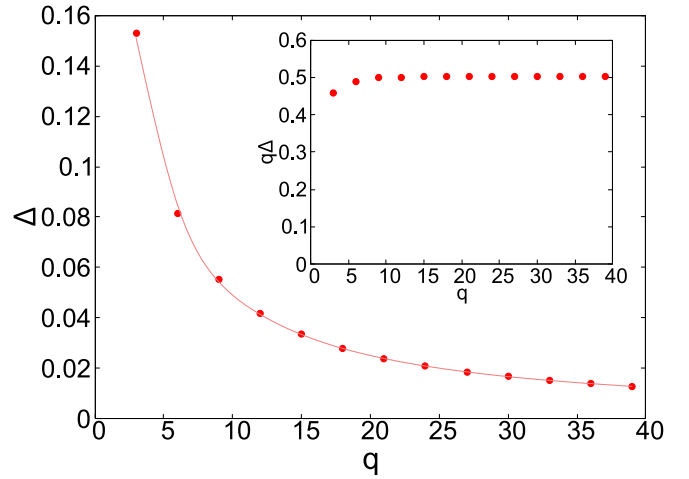


FIG. 8. Majorana excitation gap  $\Delta$  in the system with the flux configuration  $q = 3n$  with integer  $n$ . The inset shows  $q\Delta$  with respect to  $q$ .

by the toric code. When  $J_z = 0$ , the system is reduced to isolated one-dimensional spin chains composed of  $x$  and  $y$  bonds. The system is then described by the free Majorana fermions and the flux configuration is also irrelevant. In the following, we discuss how the flux configurations affect low-energy Majorana excitations in the Kitaev model away from these two limits.

### III. RESULT

We consider the triangular flux configuration to discuss Majorana excitations. Diagonalizing the Hamiltonian with the corresponding configurations  $\{\eta_r\}$  [49,50], we obtain the Majorana dispersion relations. Then, we focus on the Majorana gap  $\Delta$  given by the lowest energy of the Majorana dispersion. First, we consider the flux configuration with  $q = 1$ , where the system is fully covered by the fluxes. Now, the Majorana gap is examined under the condition with  $J_x = J_y$ , as shown in Fig. 3. When  $J_z = 0$ , the system is reduced to one-dimensional chains, where the flux configuration plays no role for the Majorana excitation and the system is gapless. Introducing  $J_z$ , the flux configuration affects low-energy properties and the gapless points change. On the other hand, the gapless excitation remains until a certain value  $(J_z)_c \sim 1.243$ . Beyond  $(J_z)_c$ , the excitation gap linearly increases. In that case, the system should be effectively described by the toric code, where the flux configuration is irrelevant. Therefore, the curve of the excitation gap is similar to that for the flux-free state, which is shown as the dashed line in Fig. 3. By performing similar calculations, we obtain the Majorana excitation gap in the parameter space with  $J_x + J_y + J_z = 3$ , as shown in Fig. 4(a). We find that the gapless ground state is realized in the isotropic case ( $J_x = J_y = J_z$ ) [39], and is stable against the small anisotropy in the exchange couplings. Similar behavior is also found in the  $q = 2$  case, as shown in Figs. 3 and 4(b). Therefore, we can say that the flux configurations play a minor role in the Majorana excitations when  $q = 1$  and  $q = 2$ . Some details of the dispersion relations in the isotropic case are discussed in the Appendix.

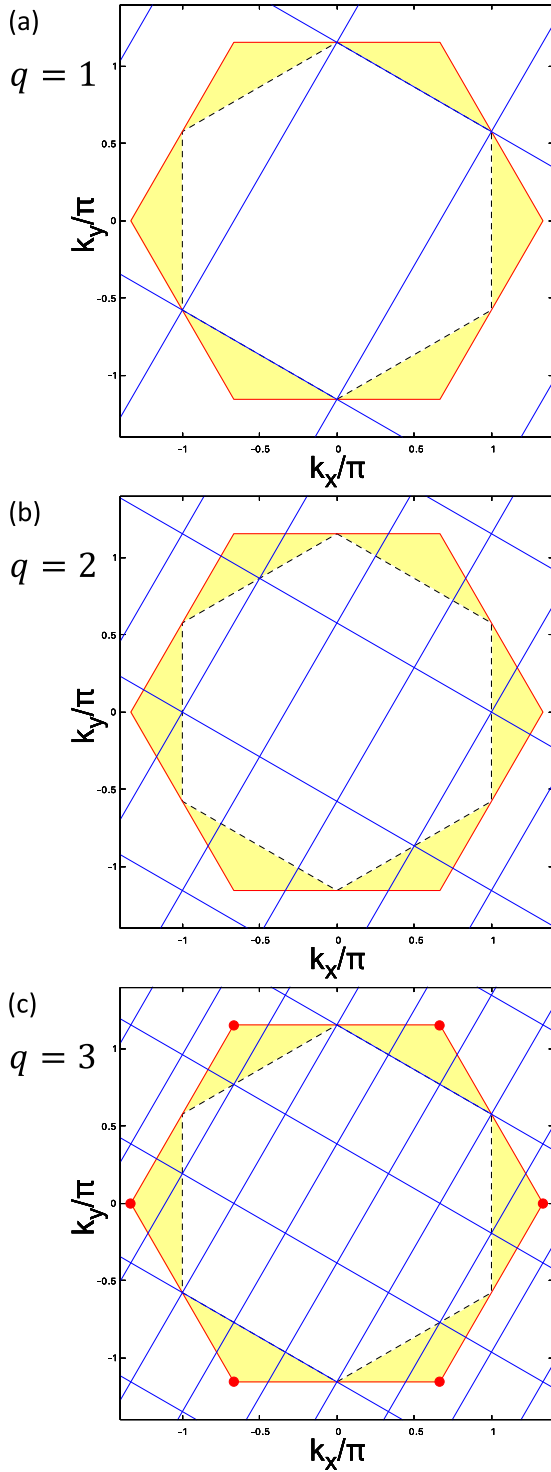


FIG. 9. Brillouin zones for the flux configurations (a)  $q = 1$ , (b)  $q = 2$ , and (c)  $q = 3$ . The shaded region shows the possible area of the gapless point  $\mathbf{k}_G$  in the flux-free system. Solid red circles at the symmetric points in the possible area are important for generating the gapped states (see text).

When  $q \geq 3$ , a distinct behavior appears in the Majorana excitations. When  $q = 3$ , we find in Fig. 5(a) the gapped state around the isotropic point. The cross section under the condition  $J_x = J_y$  clearly indicates three transition points at

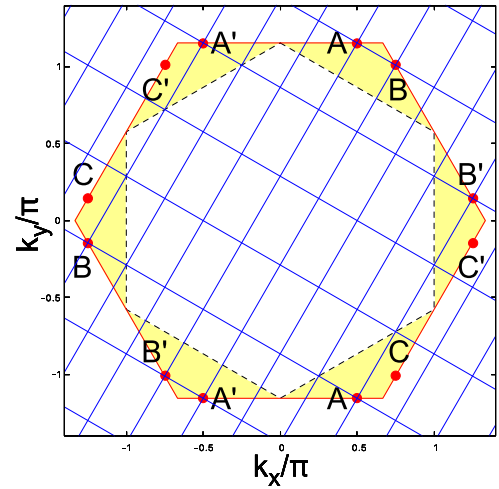


FIG. 10. Brillouin zones for the flux configuration with  $q = 4$ . Shaded region shows possible area of the gapless point  $\mathbf{k}_G$  in the flux-free system. Solid red circles at the symmetric points in the possible area are important for generating the gapped states (see text).

$J_z = 0.678, 1.308$ , and  $1.313$ , as shown in Fig. 6. This implies that, around the isotropic point, the gapped quantum spin liquid is driven by the triangular flux configuration. Furthermore, this gapped region is bounded by the gapless region although the region is narrow under the condition  $J_x = J_y$ . Therefore, we can say that this gapped state is not adiabatically connected to the gapped one realized in the large  $J_z$  limit. In the gapped state, the Majorana excitation gap takes its maximum  $\Delta = 0.153$  at the isotropic point  $J_x = J_y = J_z$ . The number of gapped states stabilized by the flux configurations is one for  $q = 3$ , three for  $q = 4$ , and six for  $q = 5$ , as shown in Fig. 5. We note that, for the cases  $q = 4$  and  $q = 5$ , the system is gapless in the isotropic point. This implies that the anisotropy in the exchange interactions as well as the flux configurations plays an important role in realizing the gapped states. The maximum of the gap is located on the axis of  $J_x = J_y$  (and its equivalent axes), and the corresponding exchanges are given as  $J_z \simeq 1.228$  for  $q = 4$  and  $J_z \simeq 0.720, 1.323$  for  $q = 5$ , as shown in Fig. 6. Figure 7 shows the Majorana excitation gap in the systems with  $q = 6, 7$ , and  $8$ . We find several gapped states in the triangular region. The number of gapped states is represented by  $(q - 1)(q - 2)/2$  for the flux configuration  $q$ . An important point is that the bilayer structure appears from the isotropic point  $J_x = J_y = J_z$ . In the case with  $q = 6$ , the gapped state is realized at the isotropic point, and away from this state (second layer), nine distinct gapped states are realized. When  $q = 7$  ( $q = 8$ ), 3 (6) gapped states appear in the first layer, and 12 (15) gapped states appear in the second layer. These results should suggest that “three” is a key role in the Kitaev system [39]. In fact, the increase in  $q$  by three increments the number of the layer, which has been confirmed in the system with the flux configurations with  $q \geq 10$  (not shown).

When  $q = 3n$  with integer  $n$ , the Majorana excitation gap appears at the isotropic point, as shown in Fig. 8. Increasing  $q$ , the Majorana excitation gap monotonically decreases. Since  $q\Delta$  is nearly constant with respect to changes in  $q$ ,  $\Delta$

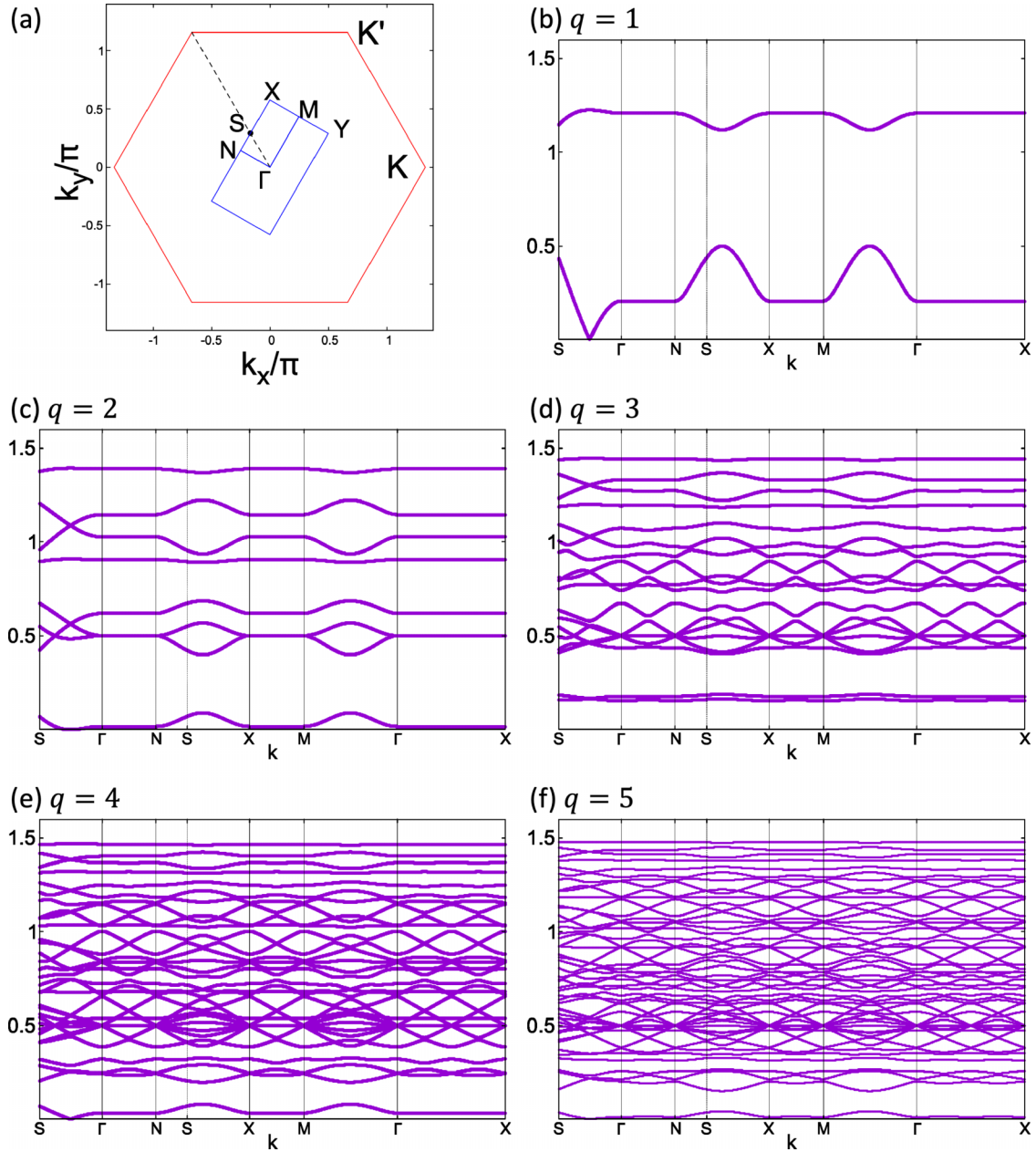


FIG. 11. (a) Reduced Brillouin zone in the Kitaev system with triangular flux configurations. The dispersion relations for the flux configurations (b)  $q = 1$ , (c)  $q = 2$ , (d)  $q = 3$ , (e)  $q = 4$ , and (f)  $q = 5$ .

is inversely proportional to  $q$ . In this case, the numbers of the layers and gapped states increase in the triangle region  $J_x + J_y \geq J_z, J_y + J_z \geq J_x, J_z + J_x \geq J_y$ . These facts should be consistent with the fact that the gapless ground state is realized there when  $q \rightarrow \infty$ .

The Majorana gap formation in the system with the triangular flux configuration may be simply explained, by taking into account the idea of the superlattice potential. In the flux-free case, the gapless point  $\mathbf{k}_G$  satisfies  $\epsilon(\mathbf{k}_G) = 0$ . Since  $\mathbf{k}_G \neq 0$ , two gapless points are given by  $\pm\mathbf{k}_G$  and are located inside certain regions, which are shown as the shaded areas in Fig. 2(b). Now, one takes into account the reduced Brillouin zone for the flux configuration, where the gapless points  $\pm\mathbf{k}'_G$  are defined in the reduced Brillouin zone. When

$\mathbf{k}'_G = -\mathbf{k}_G + \mathbf{K}'_G$ , where  $\mathbf{K}'_G$  is the reciprocal lattice vector, the periodic potential for the Majorana fermions from the flux should yield the hybridization between two branches, leading to the Majorana excitation gap. We note that the  $M$  and  $N$  points in the reduced Brillouin zone are not genuine symmetric points since we have treated the triangular flux configurations in terms of the set of  $\{\eta_r\}$ . Therefore, the gapped quantum spin liquid state should be realized when  $\mathbf{k}'_G$  is located at the high symmetric points  $X, Y$ , and  $\Gamma$ . Figure 9 shows the reduced Brillouin zones for the  $q = 1, 2$ , and 3 cases in the original hexagonal Brillouin zone with the shaded area (see also Fig. 2). We clearly find there are no high symmetric points in the corresponding regions for  $q = 1$  and 2. Therefore, the flux configuration plays a minor

role in the Majorana excitations, which is consistent with the absence of the gapped states. In the case  $q = 3$ , the region includes the  $\Gamma$  point. Therefore, around the corresponding exchanges  $J_x = J_y = J_z$ , the Majorana gap is induced, which is consistent with the numerical results. Figure 10 is the reduced Brillouin zone for the flux configuration  $q = 4$ . We find three symmetric points in the shaded area. The  $A$  ( $A'$ ) point is located at the  $X$  point, the  $B$  ( $B'$ ) point is at the  $Y$  point, and the  $C$  ( $C'$ ) point is at the  $\Gamma$  point in the reduced Brillouin zone. These three points are equivalent under the exchange operation  $\{J_x, J_y, J_z\}$ . The exchange couplings for the  $A$  point being the gapless point in the Majorana dispersion are given by  $J_x = J_y = 3 - 3/\sqrt{2}$  and  $J_z = 3(\sqrt{2} - 1)$ . The values are close to  $(J_x, J_y, J_z) = (0.886, 0.886, 1.228)$ , where the Majorana excitation takes a maximum in its gapped state. As for the  $q = 5$  case, there are two independent points under the condition  $J_x = J_y$ . When  $J_z \sim 0.708(1.342)$ , the gapless point is located at the  $\Gamma$  ( $X$ ) point in the reduced Brillouin zone. These are also consistent with the fact that the Majorana excitation gap takes a maximum in the distinct gapped states. As  $q$  increases, the unit cell of the flux configurations becomes larger while the reduced Brillouin zone becomes smaller. In this case, high symmetry points in the reduced Brillouin zone are covered by some shaded areas, which leads to the increase of the number of gapped states. The number of symmetry points in the shaded area is  $(q - 1)(q - 2)/2$ , which is consistent with the number of gapped states. For these reasons, we can say that the triangular flux configuration yields the periodic potential for the Majorana fermions and the excitation gap opens when  $k_G$  coincides with high symmetry points. It is naively expected that this can be applied to the Kitaev system with distinct flux configurations, which is now under consideration.

#### IV. SUMMARY

We have investigated the anisotropic Kitaev model with triangular flux configurations to discuss the Majorana excitation. Systematic numerical calculations have clarified how the anisotropy of the exchange couplings and flux configuration create the Majorana excitation gap. The induced gapped quantum spin liquid states are not adiabatically connected to the gapped one realized in the large anisotropic limit. Therefore, these two states are distinct from each other. We have also addressed the  $q$  dependence of the gap magnitude of the Majorana excitations. These results suggest that Majorana insulators may be realized by controlling the anisotropy in the exchanges and/or flux configurations. We believe that the realization of Majorana insulators will further advance research into the development of quantum devices using Majorana fermions.

#### ACKNOWLEDGMENTS

Parts of the numerical calculations are performed in the supercomputing systems in ISSP, the University of Tokyo.

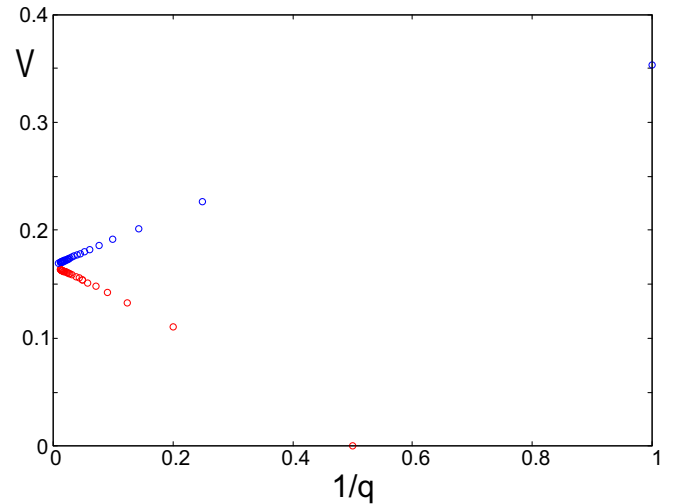


FIG. 12. The magnitude of the gradient of the Dirac cone  $V$  as a function of  $1/q$ . Blue (red) circles represent the results for  $q \equiv 1$  ( $q \equiv 2$ ).

This work was supported by Grant-in-Aid for Scientific Research from JSPS, KAKENHI Grants No. JP20K14412, No. JP21H05017 (Y.M.), No. JP22K03525, No. JP21H01025, and No. JP19H05821 (A.K.), and JST CREST Grant No. JPMJCR1901 (Y.M.).

#### APPENDIX: THE DISPERSION NEAR THE ZERO POINT IN THE ISOTROPIC CASE

Here, we discuss the Majorana excitations in the isotropic case ( $J_x = J_y = J_z$ ). In this case, the system is essentially the same as the graphene system, where the effect of the vortex configurations has been discussed [51]. The dispersion relations for  $q = 1, 2, 3, 4$ , and 5 are shown in Fig. 11. It is found that the system is gapped in the case with  $q = 3$ . On the other hand, in the others,  $q \not\equiv 0 \pmod{3}$  and the system is gapless, as discussed in Sec. III. In fact, we find that the zero-energy state always appears at the midpoint between the  $S$  and  $\Gamma$  points. Furthermore, the linear dispersion appears except for the configuration with  $q = 2$ . Figure 12 shows the velocity of the dispersion relation calculated up to the configuration  $q = 100$ , which should be important in the Majorana-mediated transport [29–31]. We clearly find that these can be divided into two groups  $q = 1$  or  $2 \pmod{3}$ , which are shown as blue and red circles. In the large  $q$  limit, each velocity approaches  $0.17J$ , which is different from that for the flux-free case  $v = \frac{\sqrt{3}}{4}J$ . Since the energy scale for the Majorana excitation originated from the flux configuration should be tiny in the large  $q$  case, the Majorana excitations are almost described by the flux-free Kitaev model except for the lowest energy states. Since the spin transport in the Kitaev model is mediated by the Majorana fermions with finite energy, a small number of fluxes has little effect on the velocity of the spin transport. The details of the phase shift (Aharonov-Bohm effect) due to an isolated flux have been discussed [38].

- [1] A. Kitaev, *Ann. Phys.* **321**, 2 (2006).
- [2] G. Jackeli and G. Khaliullin, *Phys. Rev. Lett.* **102**, 017205 (2009).
- [3] J. Chaloupka, G. Jackeli, and G. Khaliullin, *Phys. Rev. Lett.* **105**, 027204 (2010).
- [4] Y. Yamaji, Y. Nomura, M. Kurita, R. Arita, and M. Imada, *Phys. Rev. Lett.* **113**, 107201 (2014).
- [5] J. Nasu, M. Udagawa, and Y. Motome, *Phys. Rev. Lett.* **113**, 197205 (2014).
- [6] J. Nasu, M. Udagawa, and Y. Motome, *Phys. Rev. B* **92**, 115122 (2015).
- [7] T. Suzuki, T. Yamada, Y. Yamaji, and S.-I. Suga, *Phys. Rev. B* **92**, 184411 (2015).
- [8] J. Yoshitake, J. Nasu, Y. Kato, and Y. Motome, *Phys. Rev. B* **96**, 024438 (2017).
- [9] Y. Yamaji, T. Suzuki, T. Yamada, S.-i. Suga, N. Kawashima, and M. Imada, *Phys. Rev. B* **93**, 174425 (2016).
- [10] M. Gohlke, R. Verresen, R. Moessner, and F. Pollmann, *Phys. Rev. Lett.* **119**, 157203 (2017).
- [11] A. Koga, H. Tomishige, and J. Nasu, *J. Phys. Soc. Jpn.* **87**, 063703 (2018).
- [12] Y. Motome and J. Nasu, *J. Phys. Soc. Jpn.* **89**, 012002 (2020).
- [13] Y. Singh and P. Gegenwart, *Phys. Rev. B* **82**, 064412 (2010).
- [14] Y. Singh, S. Manni, J. Reuther, T. Berlijn, R. Thomale, W. Ku, S. Trebst, and P. Gegenwart, *Phys. Rev. Lett.* **108**, 127203 (2012).
- [15] R. Comin, G. Levy, B. Ludbrook, Z.-H. Zhu, C. N. Veenstra, J. A. Rosen, Y. Singh, P. Gegenwart, D. Stricker, J. N. Hancock, D. van der Marel, I. S. Elfimov, and A. Damascelli, *Phys. Rev. Lett.* **109**, 266406 (2012).
- [16] S. K. Choi, R. Coldea, A. N. Kolmogorov, T. Lancaster, I. I. Mazin, S. J. Blundell, P. G. Radaelli, Y. Singh, P. Gegenwart, K. R. Choi, S.-W. Cheong, P. J. Baker, C. Stock, and J. Taylor, *Phys. Rev. Lett.* **108**, 127204 (2012).
- [17] K. Kitagawa, T. Takayama, Y. Matsumoto, A. Kato, R. Takano, Y. Kishimoto, S. Bette, R. Dinnebier, G. Jackeli, and H. Takagi, *Nature (London)* **554**, 341 (2018).
- [18] T. Takayama, A. Kato, R. Dinnebier, J. Nuss, H. Kono, L. S. I. Veiga, G. Fabbris, D. Haskel, and H. Takagi, *Phys. Rev. Lett.* **114**, 077202 (2015).
- [19] K. W. Plumb, J. P. Clancy, L. J. Sandilands, V. V. Shankar, Y. F. Hu, K. S. Burch, H.-Y. Kee, and Y.-J. Kim, *Phys. Rev. B* **90**, 041112(R) (2014).
- [20] Y. Kubota, H. Tanaka, T. Ono, Y. Narumi, and K. Kindo, *Phys. Rev. B* **91**, 094422 (2015).
- [21] M. Songvilay, J. Robert, S. Petit, J. A. Rodriguez-Rivera, W. D. Ratcliff, F. Damay, V. Balédent, M. Jiménez-Ruiz, P. Lejay, E. Pachoud, A. Hadj-Azzem, V. Simonet, and C. Stock, *Phys. Rev. B* **102**, 224429 (2020).
- [22] Y. Kasahara, T. Ohnishi, Y. Mizukami, O. Tanaka, S. Ma, K. Sugii, N. Kurita, H. Tanaka, J. Nasu, Y. Motome, T. Shibauchi, and Y. Matsuda, *Nature (London)* **559**, 227 (2018).
- [23] T. Yokoi, S. Ma, Y. Kasahara, S. Kasahara, T. Shibauchi, N. Kurita, H. Tanaka, J. Nasu, Y. Motome, C. Hickey, S. Trebst, and Y. Matsuda, *Science* **373**, 568 (2021).
- [24] M. Yamashita, J. Gouchi, Y. Uwatoko, N. Kurita, and H. Tanaka, *Phys. Rev. B* **102**, 220404(R) (2020).
- [25] J. A. N. Bruin, R. R. Claus, Y. Matsumoto, N. Kurita, H. Tanaka, and H. Takagi, *Nat. Phys.* **18**, 401 (2022).
- [26] P. A. McClarty, X.-Y. Dong, M. Gohlke, J. G. Rau, F. Pollmann, R. Moessner, and K. Penc, *Phys. Rev. B* **98**, 060404(R) (2018).
- [27] E. Z. Zhang, L. E. Chern, and Y. B. Kim, *Phys. Rev. B* **103**, 174402 (2021).
- [28] P. Czajka, T. Gao, M. Hirschberger, P. Lampen-Kelley, A. Banerjee, J. Yan, D. G. Mandrus, S. E. Nagler, and N. P. Ong, *Nat. Phys.* **17**, 915 (2021).
- [29] T. Minakawa, Y. Murakami, A. Koga, and J. Nasu, *Phys. Rev. Lett.* **125**, 047204 (2020).
- [30] H. Taguchi, Y. Murakami, A. Koga, and J. Nasu, *Phys. Rev. B* **104**, 125139 (2021).
- [31] H. Taguchi, Y. Murakami, and A. Koga, *Phys. Rev. B* **105**, 125137 (2022).
- [32] A. Y. Kitaev, *Ann. Phys.* **303**, 2 (2003).
- [33] N. Arakawa and K. Yonemitsu, *Phys. Rev. B* **103**, L100408 (2021).
- [34] R. G. Pereira and R. Egger, *Phys. Rev. Lett.* **125**, 227202 (2020).
- [35] J. Feldmeier, W. Natori, M. Knap, and J. Knolle, *Phys. Rev. B* **102**, 134423 (2020).
- [36] M. Udagawa, S. Takayoshi, and T. Oka, *Phys. Rev. Lett.* **126**, 127201 (2021).
- [37] A. P. Joy and A. Rosch, *Phys. Rev. X* **12**, 041004 (2022).
- [38] J. Nasu, Y. Murakami, and A. Koga, *Phys. Rev. B* **106**, 024411 (2022).
- [39] A. Koga, Y. Murakami, and J. Nasu, *Phys. Rev. B* **103**, 214421 (2021).
- [40] A. Hashimoto, Y. Murakami, and A. Koga, *J. Phys.: Conf. Ser.* **2164**, 012028 (2022).
- [41] V. Lahtinen, A. W. W. Ludwig, J. K. Pachos, and S. Trebst, *Phys. Rev. B* **86**, 075115 (2012).
- [42] V. Lahtinen, A. W. W. Ludwig, and S. Trebst, *Phys. Rev. B* **89**, 085121 (2014).
- [43] J.-N. Fuchs, S. Patil, and J. Vidal, *Phys. Rev. B* **102**, 115130 (2020).
- [44] S.-S. Zhang, C. D. Batista, and G. B. Halász, *Phys. Rev. Res.* **2**, 023334 (2020).
- [45] E. H. Lieb, *Phys. Rev. Lett.* **73**, 2158 (1994).
- [46] H.-D. Chen and J. Hu, *Phys. Rev. B* **76**, 193101 (2007).
- [47] X.-Y. Feng, G.-M. Zhang, and T. Xiang, *Phys. Rev. Lett.* **98**, 087204 (2007).
- [48] H.-D. Chen and Z. Nussinov, *J. Phys. A: Math. Theor.* **41**, 075001 (2008).
- [49] F. L. Pedrocchi, S. Chesi, and D. Loss, *Phys. Rev. B* **84**, 165414 (2011).
- [50] F. Zschocke and M. Vojta, *Phys. Rev. B* **92**, 014403 (2015).
- [51] M. Kamfor, S. Dusuel, K. P. Schmidt, and J. Vidal, *Phys. Rev. B* **84**, 153404 (2011).